Nondestructive Testing and Evaluation

ISSN: (Print) (Online) Journal homepage: https://www.tandfonline.com/loi/gnte20

Detecting crack on-set time in mortar prisms with a thermal image

Jong-Gun Park, Gwanghee Heo, Jung Kim, Tetiana Venkel & Jung-Young Son

To cite this article: Jong-Gun Park, Gwanghee Heo, Jung Kim, Tetiana Venkel & Jung-Young Son (2022): Detecting crack on-set time in mortar prisms with a thermal image, Nondestructive Testing and Evaluation, DOI: 10.1080/10589759.2022.2121395

To link to this article: https://doi.org/10.1080/10589759.2022.2121395

Published online: 17 Sep 2022.

NONDESTRUCTIVE TESTING AND EVALUATION
https://doi.org/10.1080/10589759.2022.2121395

Taylor & Francis
Taylor & Francis Group

Detecting crack on-set time in mortar prisms with a thermal image

Jong-Gun Park[a], Gwanghee Heo[a], Jung Kim[a], Tetiana Venkel[b] and Jung-Young Son[a]

[a]Public Safety Research center, Konyang University, Nonsan, Korea; [b]Sciences Department, Chernivtsi University, Chernivtsi, UKraine

ABSTRACT

Thermal images are used to visualise the crack forming processes in mortar prisms under the flexural strength test with a UTM (Universal Testing Machine). The surface temperature of the prisms increases as the stress on them increases. When the prisms are reinforced by carbon fibres, the aggregated fibres along the crack paths becomes distinctive due to their higher temperature compared with their surrounding mortar areas of the prisms. This enables to visualise the crack forming process. In this process, there is a moment of abrupt increase in the temperature gradient of the aggregated fibres. This moment matches closely to that of the crack on-set obtained from the video images of crack forming process taken with a panchromatic camera, with less than 2.2 % difference. The moment is also matched with that of sharp dropping in the force from the UTM after the peak. This sudden temperature gradient increase can be used to determine the crack on-set times of the prisms with a high accuracy.

ARTICLE HISTORY
Received 22 April 2022
Accepted 31 August 2022

KEYWORDS
Thermal image; mortar prisms; carbon fibre reinforced; temperature gradient; visualising crack forming process

1. Introduction

Cracks in concrete structures are an important parameter of diagnosing the structural characteristics such as strength and durability of the structures. For this reason, the devices such as a crack microscope/Callipers and ultrasonic pulse velocity tester have been frequently used to monitor crack widening and deepening, respectively. Along with these devices, thermal image has also been used to detect the presences of cracks [1] and crack width [2] in concrete walls, cracks inside the concrete wall [3], cracks due to bond defects in CFRP (Carbon Fibre Reinforced Polymer) laminated concrete [4], and cracks in building [5], bridge [6] and infrastructure [7]. The thermal imaging is more convenient than the devices because they do not need to be closed to the cracks to be measured as the devices do. But its applications are limited only in identifying the crack presences in the structures to be tested because the thermal image can mainly find the surface temperature distribution of the object to be tested. Hence, its identifying accuracy is solely determined by the resolvable temperature difference between the crack area and its neighbours. The thermal image can be hardly used to measure the crack size because of its low sizing accuracy compared with those of the devices. This

CONTACT Jung-Young Son jyson@konyang.ac.kr

low sizing accuracy comes from the large pixel size of the thermal camera and the finite object distance from the camera. The current thermal cameras can hardly detect the cracks with openings in submillimeter because each pixel consisting of the image corresponds to more than several 100^{th} μm in current thermal imaging cameras. This is why the thermal image is only occasionally used in detecting cracks in the concrete structures. However, in this paper, it is introduced that a method of predicting the on-set time of the cracks appearing in the mortar prisms reinforced with a carbon fibre, with near 98% accuracy. The temperature distribution reveals the potential crack path even before the initiation of the crack path. This will be impossible with the devices mentioned above. The method will make the thermal image an essential diagnostic tool of monitoring cracks in the various concrete structures. The validity of the method is demonstrated in the flexural strength testing process of the mortar prisms reinforced with carbon fibres.

The flexural strength is an essential quality parameter that defines the bending property of the concrete structures including mortar prisms. To increase the strength, they are often mixed with carbon fibres [8]. Since the flexural strength test is always accompanied with a crack in the concrete structures/prisms being tested, visualising the crack forming process can help to better understand the role of the carbon fibres in the concrete structures/prisms to increase the strength. For the visualisation, both a thermal camera and a digital camera can be simultaneously used: The thermal camera converts the stresses concentrated on the object being tested to the object's surface temperature distribution. This is not possible with the digital camera. While the digital camera provides the image of a highly resolved object's profile, texture and colours in the spectral ranges of 0.4 to 0.9μm. The digital camera is also called a panchromatic camera. The commercially available thermal camera covers one of the three infrared wavelength ranges of 1.4 μm to 2.4 μm, 3.0 μmto 5.0 μmand 7.5μm to 14μm [9,10]. And the temperature distribution is represented by pseudo-colours on the object's profile. So, the simultaneous use of both the panchromatic and the thermal cameras will enable to obtain a highly resolved object image with its surface stress distribution. This can help to identify with a high accuracy the locations of the defects and inhomogeneities formed by physical, chemical or physicochemical processes in the object.

In this paper, a method of determining the on-set time of the cracks in fibre-reinforced mortar prisms with a thermal image is introduced, and the process of crack development in the prisms and the role of carbon fibres in the process are visualised, when the prisms are under stress by a UTM (Universal Testing Machine) [11] for testing their flexural strengths.

2. Mortar prism sample preparation and experimental set-up

To prove thermal image's capability of visualising the process of crack formation in the flexural strength measurements, many prisms having the shape of a rectangular parallelepiped with the sizes of 160 mm (length) x 40 mm (width) x 40 mm (Height) with or without carbon fibres are prepared. The prisms with fibres and no fibres, i.e. plain prisms are prepared by the instructions shown in KS L ISO 679(2016). The plain prisms are

made from a mortar that is a mixture of cement powder, standard sand with the ratio of cement:sand:water = 1:3:0.5 in weight without admixture.

To make the mortar, the cement and sand are being mixed first for 60 seconds then water is poured to them and mixed together for 150 sec. The mortar is cast to the prism shape for 24 hours and then it had been kept in a water tank with constant temperatures of 20℃ ± 2℃ for 28 days for curing. Three plain mortar prisms are prepared in this way. For the prisms with carbon fibres, the cement and sand are mixed first for 1 min and then the fibres are added to the mixture and mixed together for 90 seconds. On this mixture, water (50% of the cement weight as above) and admixture (polycarboxylate superplasticizer, 1.0% of the cement weight) are poured to the mixture, and mixed again for 150 seconds. The casting and curing processes are the same as for the plain prisms.

The cement is the general-purpose ordinary Portland cement; the sand has the particles sizes of not greater than 2 mm in diameter; each fibre strand has the diameter of 7 ± 2 μm and the tensile strength of 4,900 MPa. The strand is made of twisting 12,000 fibres together and then it is cut to the length of 6 mm. The fibre amounts added to the cement and sand mixture are 0.5%, 1.0% and 1.5% and 2.0% in volume of the total volume of the mortar. two mortar prism samples are made for each percentage. If the plain prisms are included, 10 prisms are made in total. The 10 prisms are identified as CF 0.0-1(2), i.e. plain prisms, CF 0.5-1(2), CF 1.0-1(2), CF 1.5-1(2) and CF 2.0-1(2). CF represent initial letters of carbon fibre, the numbers in the middle – carbon fibre percentages and the last digit is the sample number. The last digit is often omitted to represent both samples together. The weight of each prism is measured as 0.5 kg.

For the flexural strength measurement of the prisms, a UTM is used, which can press the testing prism up to 400 KN/m^2. The machine has a three-axle configuration, i.e. three axles aligned in parallel for mounting and applying stress for the rate of 3 KN/min to the prism sample. The two bottom axles are distanced 120 mm and the top axle is in the middle of the two bottom axles, but above the two axles, corresponding to the height of the prism. The distance between the top and the bottom axles can be controlled to fit the prisms' heights.

To observe the crack forming process, a panchromatic camera, Nikon D-5, which has a pixel size and resolution of 6.45 μm and 5568 x 3712, respectively. The crack on-set time is determined with a high accuracy in the observing the process. The camera allows taking a video image with the resolution of 3840 x 2160 and the frame rate of 24 frames/sec [12]. The camera distance from the prism is set to 1.0 m from the normal direction of the prism sample to fill its image detector with the prism image as much as possible, especially in the horizontal direction. The distance allows 3,770 pixels in video mode to cover the horizontal size of each prism, i.e. 160 mm. Hence, each pixel corresponds to 42.5 μm of the prism surface.

Along with the panchromatic camera, a thermal camera FLIR T640, which has a pixel size of 17 μm, pixel resolution of 640 x 480, temperature resolution of 0.03°K at 30°C and operating in the wavelength range of 7.5μm to 14μm, is also set to the same distance as the panchromatic camera. It is also adjusted to make the prism image to cover almost all the area of the thermal camera's image detector in horizontal direction with use of its zooming capability. As a result, 624 x 156 pixels are assigned for the prism image. So,

each pixel covers 0.2564 mm (160 mm/624) x 0.2564 mm (40 mm/156) of the prism surface area. The distance between two cameras is 18 cm. They are aligned symmetrically along the normal line of the prism sample. The viewing angle of each camera is about 5°. This angle causes almost unnoticeable image distortion between left and right sides of the prism image because the distance of the camera to either left and right most side of the prism cannot exceed 1.015 m for both cameras. The thermal camera allows taking a video image with 30 frames/sec rate.

The experimental set-up is consisted of a UTM with a testing prism mounted on it and two cameras as shown in Figure 1. The images from the two cameras for the prism in test are also shown. The shutters of the two cameras are working synchronously with the time of applying stress to the prism from the UTM to taking the video images of the prism under increasing forces for determining the flexural strength of the prism and observing the process of the crack forming in it. However, there can be at most 3 seconds shuttering time delay between the machine and cameras because each device is operated by an assigned operator. It is expected that the occasional camera shuttering error by the camera operators can induce the shuttering time difference between two cameras to up to 2 seconds within this time delay.

3. The prism's temperature increases by the applied stress

The prism mounted on three-point bending set-up of a UTM for flexural strength testing will experience deformation that will be more from the top to bottom surfaces. The

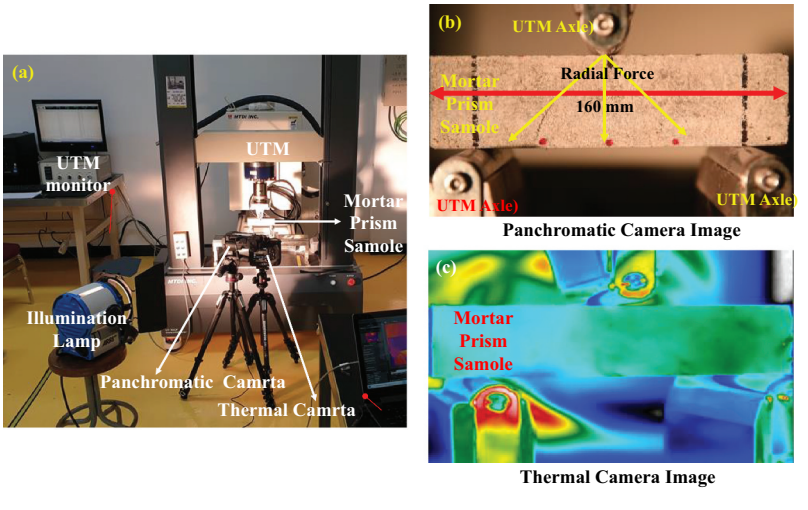

Figure 1. Experimental set-up and images from the two cameras: (a) the experimental set-up is consisting of a UTM, a Panchromatic camera. A thermal camera and an illumination lamp which illuminates the mortar prism sample mounted on the UTM axle for test. (b) the panchromatic camera image of the sample prism. Three axles (one top in the mid part of the prism sample and two bottom in the near left and right edges of the prism are also shown. The force direction specified by three arrows and the horizontal length of the prism specified with a both side arrow, are also shown. (c) the thermal image of the prism, the three axles and surrounding objects and scene shown in the panchromatic image. Each color in the image has its corresponding temperature. The color temperature increases from blue, green, yellow and red orders.
Experimental Set-up and images from the two cameras. (a) The experimental set-up. (b) The panchromatic camera image. (c) the thermal image of the prism.

bottom surface will be deformed the most for the stress imposed. Due to the increasing deformations, the defects in the prism will also be strained more while going from top to bottom surfaces. The increasing forces will further reduce the radii of curvature of the top and bottom surfaces. The prism will be broken, i.e. a crack will appear on it, if it can no longer sustain its strain incurred by its radii of curvature decrease. Since the tensile strength at bottom is much lower than the compressive strength on top, the crack will start from the bottom to the top surface. The force initiating this crack is defined as the flexural strength of the prism. As the crack progresses more, the prism will be broken into two parts.

The flexural strength can be higher when there are defects that have a higher tensile strength than the prism's main body, i.e. a mortar. When there are defects such as carbon fibres, especially, along the paths of cracks in the prism, the strength will be increased much more, because of the fibre's much higher tensile strength compared with that of the mortar and the fibres' strong adherence to the mortar. In fact, the tensile strength of the fibre 4.9 GPa is much higher than that of the concrete, which is typically in the range of 1.5 to 2.5 MPa. Hence, the fibre will resist to the stress that forces to reduce the radii of curvature of both top and bottom surfaces of the prism. When the crack started, the fibres along the crack path will be strained more because all the stresses given by the machine are now mostly applied to them.

As the crack size increases, all stresses from the machine will eventually be applied to fibre. As a result, the temperature of the fibres become higher than that of the mortar area of the prism. The strain in the fibres will increase until they are torn apart and/or detached completely from the mortar parts of the prism due to the widening of the crack gaps. This will make the fibre presence in the surface of each prism more visible. Furthermore, the sudden increase in the stress on the fibres at the moment of the crack on-set will induce the abrupt increase in the temperature gradient of the fibres. Hence, the thermal image allows visualising the defect presences more clearly, as well as the process of the crack forming by the temperature difference induced by different stresses between defects and the mortar part of the prism.

Since the stress is the amount of force exerted per unit area, it is transformed into energy per unit of volume. Hence q and the stress are not different to each other. When an energy, q in J(Joule) per unit volume is given to an object, the object will experience its temperature increase $\Delta T = T_2 - T_1$ in °K (absolute temperature), where T_1 and T_2 are object temperature before and after applying forces. $\Delta T$is expressed as,

$$\Delta T = \frac{q}{hm} \tag{1}$$

where h and $m$represent specific heat in unit of J/(kg·°K) and mass in unit of kg, of the object, respectively. For the case of UTM, q, i.e. stress is a function of time t because the force from the UTM is time varying. ΔT is also time varying. And also the actual force delivered to the prism in three axle configuration is much reduced by the factor $1.5l/wz^2$, where l represents the distance between two bottom axles of the UTM, w and z, the width and height of the prism, respectively, compared with the force from the UTM [13]. Therefore, when $x(t)$kNforce is delivered to a prism by the UTM, the temperature increase in prism will be expressed as,

$$\Delta T = \frac{1.5l}{hmwz^2} x(t) \tag{2}$$

The prisms have $m = 0.5$kgand $h = 800\text{J}/(\text{kg} \cdot °\text{K})$. With the dimension of the prisms and the UTM's axle configuration as specified above, ΔT is calculated as $(4.5x(t)/6400)°$ K, by Equation (2). However, actual ΔTcan be smaller than the calculated value due to prism's heat loss to the surrounding space when the ambient temperature is lower than that of the prism.

4. Experimental results

When forces of increasing with time are applied to each prism in the experimental set-up shown in Figure 1, the surface temperature variations of the prisms, with time are visualised as shown in Figure 2. The numbers in bottom of each image are the frame numbers in the video sequence. The time in second corresponding to the frame number is obtained by dividing the number by 30, i.e. the frame rate of the thermal camera as mentioned before. In measuring temperatures of objects with a thermal camera, the emissivity of each material should be known. However, the thermal camera in this experiment has the default emissivity value of 0.98 which is for human skin [14]. Hence the temperature value of the prisms should be modified according to the emissivity of each object forming the prisms. The emissivity of concrete and carbon fibre are known as 0.92 and 0.8, respectively. Since the transform of thermal energy to temperature is inversely proportional to emissivity to the power of 0.25, i.e. $(\text{emissivity})^{0.25}$ [14]. The temperature values should be modified by multiplying $1.052(0.98^{0.25}/0.8^{0.25})$ for carbon fibre and 1.016 $(0.98^{0.25}/0.92^{0.25})$ for mortar parts. But the temperature values in following figures are not modified because the numbers are small, and the temperature gradient that is the ratio of two consecutive temperature values is not affected by the multiplication. The effects of the thermal reflections from the objects near the prism samples are also not considered due to the same reasons above. The surface temperature variations in CF 0.0-1, CF 0.5-1, CF 1.0-1, CF 1.5-2 and CF 2.0-1 prisms are converted to pseudo colours as shown in Figure 2. The colour bar on the right side of each prism image specifies their matching temperatures. Each prism image consists of seven different video frames from the thermal camera while applying forces to the prism.

The images inform that 1) the surface temperature distribution of higher frame numbers is higher than that of lower frame numbers. 2) the surface temperatures distribution is fairly uniform for the plain prisms but the uniformity is deteriorating as the fibre percentage increases, and 3) the colour bars inform that the total temperature variation in the prisms is 4.4° for CF 0.0-1 and CF 0.5-1, 7.1° for CF 1.0-1, and 10.6° for CF 1.5-2 and CF 2.0-2. From these facts, it is concluded that 1) the fibre is an inhomogeneous material to the mortar. That is why the uniformity of the temperature distribution are worsened more as the fibre percentage increases, 2) the higher temperature regions in each prism are the places where the fibres are aggregated, and 3) the high-temperature regions within the broken rectangular are the aggregated fibres along the crack path. The temperature increase with increasing frame numbers describes more distinctively the crack paths. as shown in CF 1.5-2. The temperature distribution within the broken rectangle in the top image of CF 1.5-2 reveals almost exactly the crack path as

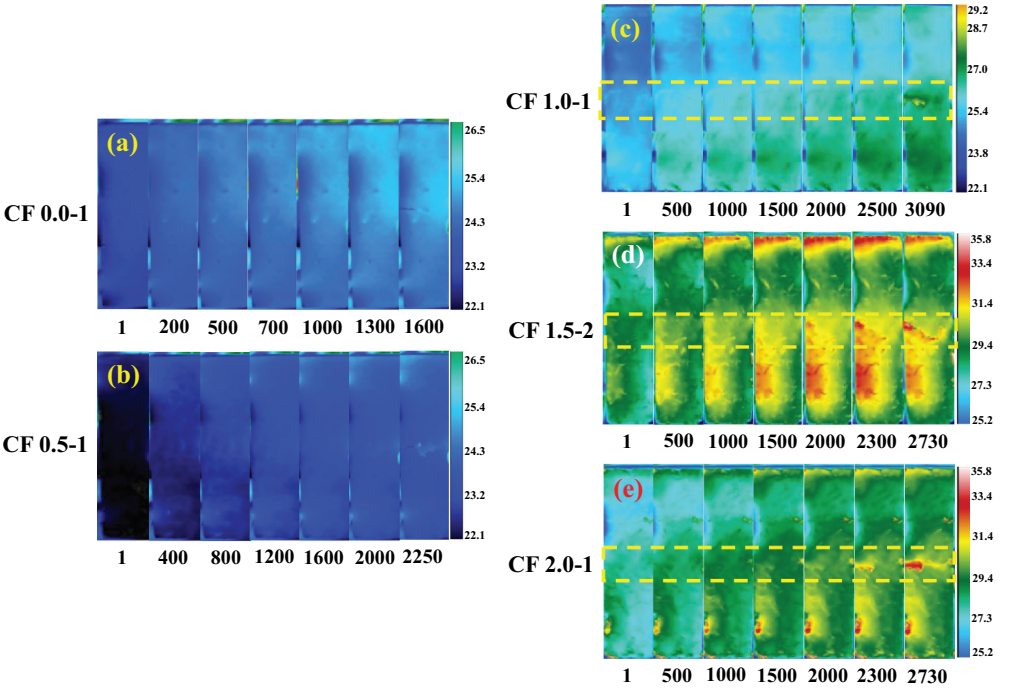

Figure 2. Surface temperature variations in prisms with time in the process of the flexural strength testing. The numbers in bottom of and the right most side of each image represent frame numbers and the temperature corresponding to each image, respectively: (a) is for CF 0.0-1. The surface temperature increases only 4.4°(22.1° to 26.5° during the 53 (1600/30(frame rate of thermal camera)) seconds period. (b) is for CF 0.5-1. The surface temperature increases the same as the CF 0.0-1 but this increase is resulted after 75 (2250/30(frame rate of thermal camera)) seconds testing. (c) is for CF 1.0-1. The surface temperature increase is 7.1°. This increase is obtained after 103 (3090/30) seconds testing. As shown in the broken rectangle which represents the crack path, the temperature increase is obtained along the crack path. The other part of the prism has nearly the same temperature increase as the previous samples. (d) is for CF 1.5-2. The surface temperature increase is 10.6°. This increase is obtained after 91 (2730/30) seconds testing. As shown in the broken rectangle which represents the crack path, the highest temperature appears along the crack path. Some parts of the surface also show high temperatures. These parts are mostly having the fibers. (e) is for CF 2.0-1. The surface temperature increase, the time of reaching the temperature are the same as CF 1.5-2. As shown in the broken rectangle which represents the crack path, the highest temperature appears along the crack path. Some parts of the surface also show high temperatures. These parts are mostly having the fibers.
Specified prisms' surface temperature variations with time in the process of the flexural strength testing. The numbers in bottom of and the right most side of each image represent frame numbers and the temperature corresponding to each color, respectively. (a) CF 0.0-1. (b) CF 0.5-1. (c) CF 1.0-1. (d) CF 1.5-2. (e) CF 2.0-1.

shown in later figures. The aggregated fibres along the path are stressed more than their neighbours. The highest temperature appears at near the bottom of the prism, where an aggregated fibre bundles is located. This is because the prism will be more deformed, i.e. more stressed as close to its bottom. Hence, the temperature distribution clearly reveals the crack forming process. This informs that the crack forming process can be visualised by the thermal image. In CF 1.5-2, the path that will be cracked, is clearly shown from

2300th frame which corresponds to 77 sec. The crack on-set time estimated by the panchromatic camera, 78 seconds indicates that the crack path will be estimated at least 1 second before the starting of the actual crack.

The time variations of forces applied to each prism by the UTM when it is set to 3 KN/min rate are shown in Figure 3. Figure 3 shows the time variation of the applied forces to each prism. The waveforms made by the variations are not the same for each prism, except a piecewise linearly increasing range. The most differences in the waveforms of different prisms lie in the highest force values and the time period of the actual force

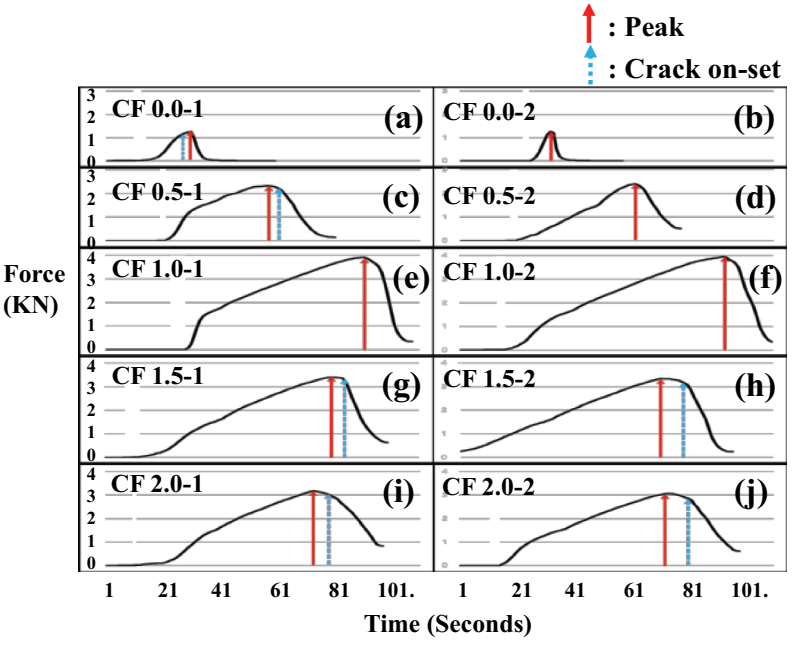

Figure 3. Force waveforms from UTM for different prisms. The horizontal and vertical axes are for time in second and applied force by the UTM in KN (Kilo Newton), respectively: (a) is the force waveform for CF 0.0-1 prism. The crack on-set time specified by the broken arrow appears before the peak force time specified by the solid arrow. (b) is the force waveform of CF 0.0-2 prism. The crack on-set time matches with the peak force time specified by the solid arrow. (c) is the force waveform of CF 0.5-1 prism. The crack on-set time specified by the broken arrow appears after the peak force time specified by the solid arrow. (d) is the force waveform of CF 0.5-2 prism. The crack on-set time matches with the peak force time specified by the solid arrow. (e) is the force waveform of CF 1.0-1 prism. The crack on-set time matches with the peak force time specified by the solid arrow. The peak force in near 4 KN and is recorded at 86 second. (f) is the force waveform of CF 1.0-2 prism. The crack on-set time matches with the peak force time specified by the solid arrow. The peak force in near 4 KN and is recorded at 88 second. (g) is the force waveform of CF 1.5-1 prism. The crack on-set time specified by the broken arrow appears after the peak force time specified by the solid arrow. (h) is the force waveform of CF 1.5-2 prism. The crack on-set time specified by the broken arrow appears after the peak force time specified by the solid arrow. (i) is the force waveform of CF 2.0-1 prism. The crack on-set time specified by the broken arrow appears after the peak force time specified by the solid arrow. (j) is the force waveform of CF 2.0-2 prism. The crack on-set time specified by the broken arrow appears after the peak force time specified by the solid arrow.

Force waveforms from UTM for the specified prisms. The horizontal and vertical axes are for time in second and applied force in KN (Kilo Newton), respectively. (a) CF 0.0-1. (b) CF 0.0-2. (c) CF 0.5-1. (d) CF 0.5-2. (e) CF 1.0-1. (f) CF 1.0-2. (g) CF 1.5-1. (h) CF 1.5-2. (i) CF 2.0-1. (j) CF 2.0-2.

delivered to each prism. The highest force value for each prism is supposed to represent the flexural strength but it is not completely matched with the crack on-set time obtained with the two cameras as will be seen later.

According to Figure 3, the peak force (Total force) applied to each of CF 1.0-2, CF 1.0-1, CF 1.5-1, CF 1.5-2, CF 2.0-1, CF 2.0-2, CF 0.5-2, CF 0.5-1, CF 0.0-2 and CF 0.0-1 is in the descending order of 3.964 KN (206.2 KN), 3.919 KN (191.79 KN), 3.402 KN (156.58 KN), 3.336 KN (170.14 KN), 3.183 KN (146.35 KN), 3.078 KN (151.32 KN), 2.407 KN (64.88 KN), 2.317 KN (78.51 KN), 1.269 KN (6.8 KN) and 1.269 KN (12.37 KN), respectively. This order informs that both peak and total forces are descending in the order of CF 1.0, CF 1.5, CF 2.0, CF 0.5 and CF 0.0, but the total forces do not correspond to the peak force order for CF 1.5, CF 2.0, CF 0.5 and CF 0.0. The prisms CF 1.5, CF 2.0 and CF 0.5 reveal that the peak force is high but total force is low or vice-verse. For the CF 0.0, the peak is the same but the total force is almost two times of those of CF 0.0-2. These order mismatches between the peak and the total forces may not have any serious meaning, because since the waveforms of different prisms do not have the same slopes and shapes, the peak force may not correspond to the total force. Moreover, the force from UTM is actually delivered to the prisms at 23.7 sec, 16.7 sec, 15.8 sec and 12.1 sec later than the force on-time of the UTM, for CF 0.0-2, CF 0.5-1, CF 1.0-1 and CF 2.0-2, respectively. However, even with this late force initiation, the temperature increase in each prism starts from the force on-time of the UTM as shown in Figure 4. This will also be a reason of why the peak and total forces do not correspond to each other. Figure 4 shows the surface temperature increase in CF 1.5-2 and CF 2.0-2 prisms, induced by the applied force. To show the surface temperature increase, the surface of each prism is divided into eight 20 mm $\times$ 40 mm regions, and then the temperature variation of each region's central point is plotted for power on period of the UTM. Added on these 8 points, the four crossing points of the horizontal bisector line of the prism and the line connecting the centre points of two vertically bounded regions, are also measured for the same period. Each point corresponds to three pixels. When these points are in the aggregated places of fibres in the prism surface, the points are moved to the mortar areas within their regions. Furthermore, the points showing highly unstable temperature variations are replaced by other points. The locations of the 12 points in each prism is specified in Figure 4. The temperature increase is calculated by finding the temperature difference between the starting and the highest temperature in each point and then averaging all 12 point values for each prism. The average values obtained this way are summarised in Table 1. For the comparison, the expected temperature increases calculated from Equation (2) at the highest force value for each prism are also shown in Table 1.

Figure 4 shows that the temperature of CF 2.0-2 increases immediately after the UTM starting like the CF 1.5-2 which starts with 0.268 KN at the very moment of the UTM starting, as shown in Figure 3. All other prisms show the same behaviours as the CF 2.0-2, though they have different forces on-times. Furthermore, the temperature increment of each point in each prism is very similar to those of other points in the same prism. This implies that the force waveforms may not correctly represent the forces actually applied to prisms, and the forces from the UTM are uniformly heating the entire prism to increase the temperature of its every point equally, though each point temperature is different from others. This is why the time variation of each point's temperature

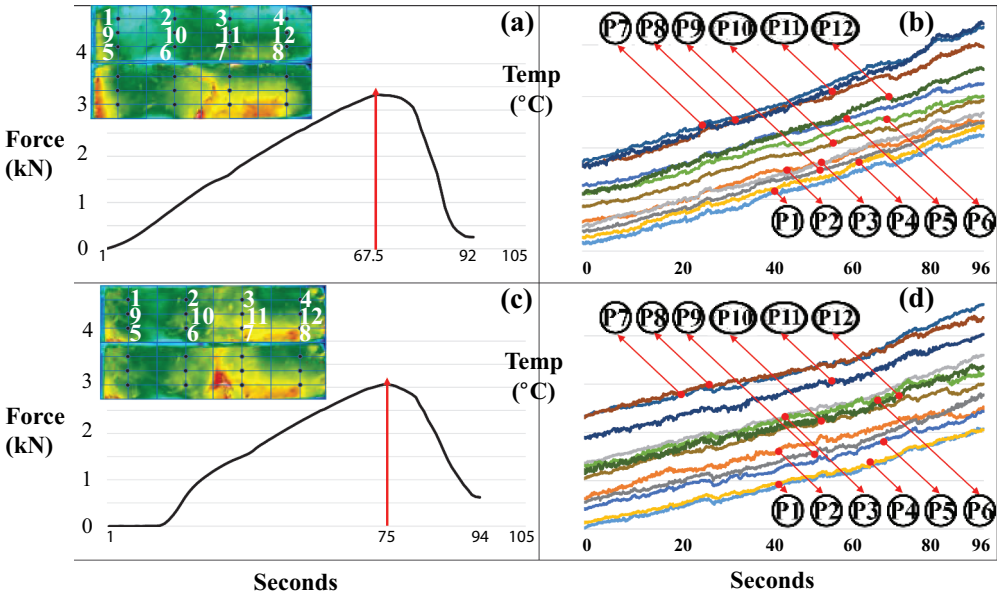

Figure 4. Temperature variations at the points specified in thermal images. The force waveforms of CF 1.5-2 and CF 2.0-2 are also given to show the prism surface temperature increase during the force on-time of UTM. The temperature increases even with no actual force for CF 2.0-2. (a) shows the thermal image in its top left side and the force waveform of CF 1.5-2. The peak force position is also specified by the solid arrow. (b) shows the time variation of the temperature at the points specified by the numbers in the thermal image at figure (a). The time variation curve of a point are almost parallel to those of other points. (c) shows the thermal image in its top left side and the force waveform of CF 2.0-2. The peak force position is also specified by the solid arrow. (d) shows the time variation of the temperature at the points specified by the numbers in the thermal image at figure (c). The time variation curve of a point are almost parallel to those at other points.

Temperature variations at the points specified in thermal images of CF 1.5-2 and CF 2.0-2: (a) The thermal image in its top left side and the force waveform of CF 1.5-2. (b) The time variation of the temperature at the points specified by the numbers in the thermal image in figure (a). (c) The thermal image in its top left side and the force waveform of CF 2.0-2. (d) The time variation of the temperature at the points specified by the numbers in the thermal image at figure (c).

distribution has almost the same shape as those of other points. However, the temperatures of the carbon fibre aggregated areas are much higher than those of the points, as shown in Figures 2 and 4. The temperature increases incurred by the forces given in Figure 3 are measured as 0.5°, 1.66°, 2.03°, 2.1° and 2.27° for CF 0.0-1, CF 0.5-1, CF 1.0-1, CF 1.5-2 and CF 2.0-1, respectively as listed in Table 1. But the ΔT calculated from Equation (2) are 1.335°, 1.629°, 2.754° 2.392° and 2.238° for the order of prisms specified above. For the case of CF 1.0-1 and CF 2.0-1, the measured $\Delta T$is higher than the calculated $\Delta T$by 0.03°. Except these two samples, the calculated ΔTvalues are higher than their corresponding measured values. Since the 0.03° is the resolution limit of the thermal camera, it can be considered as an uncertainty introduced by the thermal camera. This means that the calculated ΔT rather accurately predicts the measured one. For the cases of plain prisms, the calculated values are almost 3 times greater than their measured values, but for the carbon fibre prisms, the calculated values are mostly

Table 1. Summarised experimental results: CF is omitted in prism names.

	PM	0.0-1	0.0-2	0.5-1	0.5-2	1.0-1	1.0-2	1.5-1	1.5-2	2.0-1	2.0-2
UTM	Peak time (sec)	28.7	30.7	53.9	57.4	87.0	89.0	74.9	67.5	70.0	70.1
	Forces (KN)	1.269	1.269	2.317	2.407	3.919	3.964	3.402	3.336	3.183	3.078
	Accumulated Forces (KN)	12.37	6.8	78.51	64.88	191.79	206.2	156.58	170.14	146.35	151.32
	Temp. (° K)	1.335	1.013	1.629	1.644	2.756	2.787	2.392	2.346	2.238	2.164
Panchromatic	Crack On-Set Time (sec)	26.0	31.0	56.0	59.0	87.0	88.0	80.0	78.0	75.0	77.0
Thermal	ACT (sec)	x	x	58.1	x	86.2	90.9	81.6	79.6	71.8	77
	Temp. Increase (° K)	0.50	0.48	1.66	1.21	2.03	2.15	2.1	2.21	2.27	2.07

ACT: Time of abrupt temperature change, Temp.: Temperature, PM: Prism Name.

higher than the measured ones. The differences are in the range of 0.09° to 0.72°. The answer to these mismatches is not found yet.

The crack opening for each prism corresponding to the forces in Figure 3 is plotted in Figure 5 in terms of crack developing time (Horizontal axis) vs. crack opening (vertical axis). The crack on-set time corresponds to the crack opening of a pixel gap, i.e. 42.5 μm. The crack progressing time is found from the video images of the panchromatic camera. The crack initiation and further widening for sample prisms are shown in Figure 5. It clearly shows that 1) the on-set times of cracks for prisms with different carbon fibre percentages show discriminable differences between them, though CF 1.5 and CF 2.0 reveal a small difference compared with others, 2) the crack opening widening after the initiation of the cracks does not require much time, i.e. much forces. The crack opening widening time increment for each prism is small enough to cause its slope to be almost parallel to those of the other prisms. The carbon fibre percentage is no longer effective in blocking the further breaking of the prisms, once the crack started.

As shown in Figure 3, the on-set time specified by the dotted arrow (the time at the peak force specified by solid arrow), corresponding to CF 1.0-2, CF 1.0-1, CF 1.5-1, CF 1.5-2, CF 2.0-2, CF 2.0-1, CF 0.5-2, CF 0.5-1, CF 0.0-2 and CF 0.0-1 are 88 (88.3), 87 (86.2), 80 (74.9), 78 (67.5), 75 (70), 77 (70.1), 59 (57.4), 56 (53.9), 31 (30.7) and 26 (28.7) seconds, respectively. The time differences between the crack on-set and peak force are mostly less than 5 seconds: For CF 1.0-1(2) and CF 0.0-2, they match to each other within less than 1 second. However, CF 2.0-1 and CF 1.5-2 show around 7 seconds and 10.5 seconds differences, respectively. The large time differences are considered that they are caused by the near flat top shapes of the force waveforms. The force dropping after the

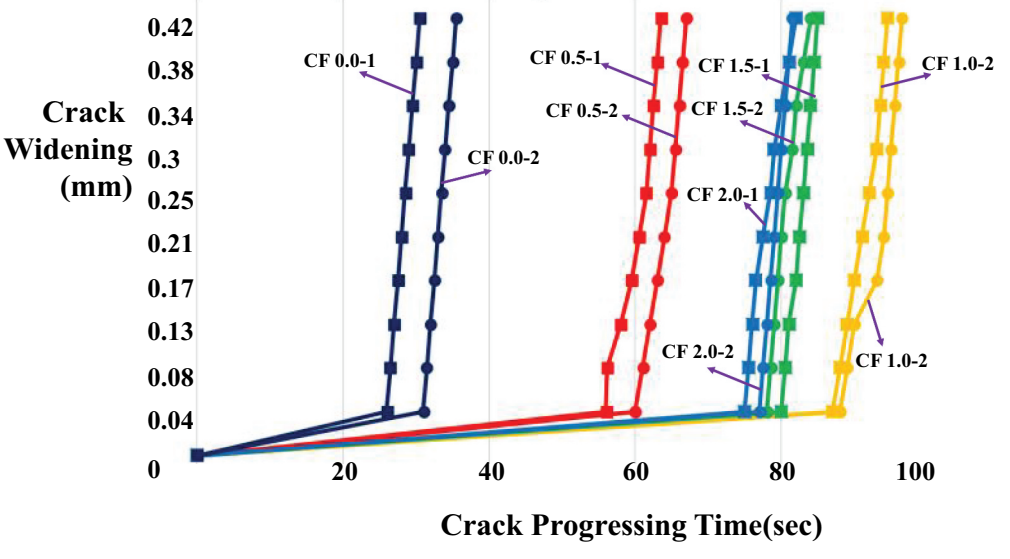

Figure 5. Crack on-set and further widening times of 10 prisms. The crack on-set time corresponds to the crack opening of a pixel gap, i.e. 42.5 μm. The time becomes longer in the order of CF 0.0, CF 0.5, CF 2.0, CF 1.5 and CF 1.0.
The crack on-set time corresponds to the crack opening of a pixel gap, i.e. 42.5 μm and further widening times of the named prisms.

peak forces is very rapid for CF 1.0 and CF 0.0-2, but very slow for CF 1.5 and CF 2.0. When prisms are cracked, the force from the UTM will drop rapidly because the resistance from the prisms is much reduced. Hence, the flat tops imply that the prisms are not cracked yet, even after the peak force.

From the force waveforms, the time taken to go down to 95% of its peak force is 3 seconds for CF 0.0-1, 1 second for CF 0.0-2, less than 3 seconds for CF 1.0 and CF 0.5, 5 seconds for CF 1.5-1 and CF 2.0-1, 6 seconds CF 2.0-2 and 8 seconds for CF 1.5-2. These times inform that as the prisms have larger time differences, the flat top time periods are also increased in proportional to the differences. Hence if this flatness is considered, the times at the peak forces, 74.9 (CF 1.5-1), 67.5 (CF 1.5-2), 70 (CF 2.0-1), 70.1 (CF 2.0-2), 28.7 (CF 0.0-1), and 53.9 (CF 0.5-1) seconds can be adjusted as 80, 76, 75, 76, 26, and 58 seconds, respectively. These adjusted times match with the measured on-set times, with 2 seconds difference at most. This means that the cracks in prisms do not always start with the peak forces, but they rather start at the points, where the forces in the waveforms drop sharply. This sharp dropping point for the prisms with the flat top waveforms will indicate the crack on-set. The time required to on-setting the crack is increased in the order of CF 0.0, CF 0.5, CF 2.0, CF 1.5 and CF 1.0. This order matches with the order of the peak forces applied to the prisms. This informs that the reinforcing of mortar prisms with carbon fibres makes the flexural strength increase. But too much addition can reduce the strength due to the increased inhomogeneity of the prisms [15].

As mentioned before, the temperatures of the aggregated fibre bundles along the crack paths increase more than those of the mortar parts as shown in Figure 6. Figure 6 shows the comparison between the crack images in panchromatic and thermal cameras at the times of the crack on-set (left side) and the near vanishing moment of forces from UPM (the widened crack opening in right side), for all prisms. The top and bottom images in each prism are the panchromatic and thermal images, respectively. The left-side panchromatic and thermal images comprise the crack image at the crack on-set time. The small and large solid boxes in the panchromatic image specify the crack with a pixel width and its magnified image, respectively. The right-side panchromatic and thermal images show the widened crack openings. These images show that the crack paths are continuous for the prisms with no carbon fibres but they are broken for those with carbon fibres. The broken parts along the crack path, specified by dotted line boxes are identified as the aggregated carbon fibre bundles of various shapes because they appear as higher temperature areas in the thermal images. The bundles are either on or slightly underneath of the prism surface. The cracks cannot cross the bundles directly because of the bundle's resistance to the deformation of the prism. Hence the thermal images show the presences of the carbon fibre bundle along the crack path and their temperature variation during the crack forming and widening. The arrows indicate the matching areas in the thermal image to the boxes in its corresponding panchromatic image.

The boxed area in CF 0.5-2, shows clearly the presence of a broken part in the crack path, but no discriminable temperature increase is spotted in its thermal image. This means that the carbon fibre bundles inducing the broken part are either too small to cause local heating that will induce a resolvable temperature difference with its neighbours or underneath of the surface. In other carbon fibre added prisms, the area is further divided into several sub-areas that are discriminated by several different colours such as blue, green, yellow, red and white. The colour boundaries of discriminating the sub-areas

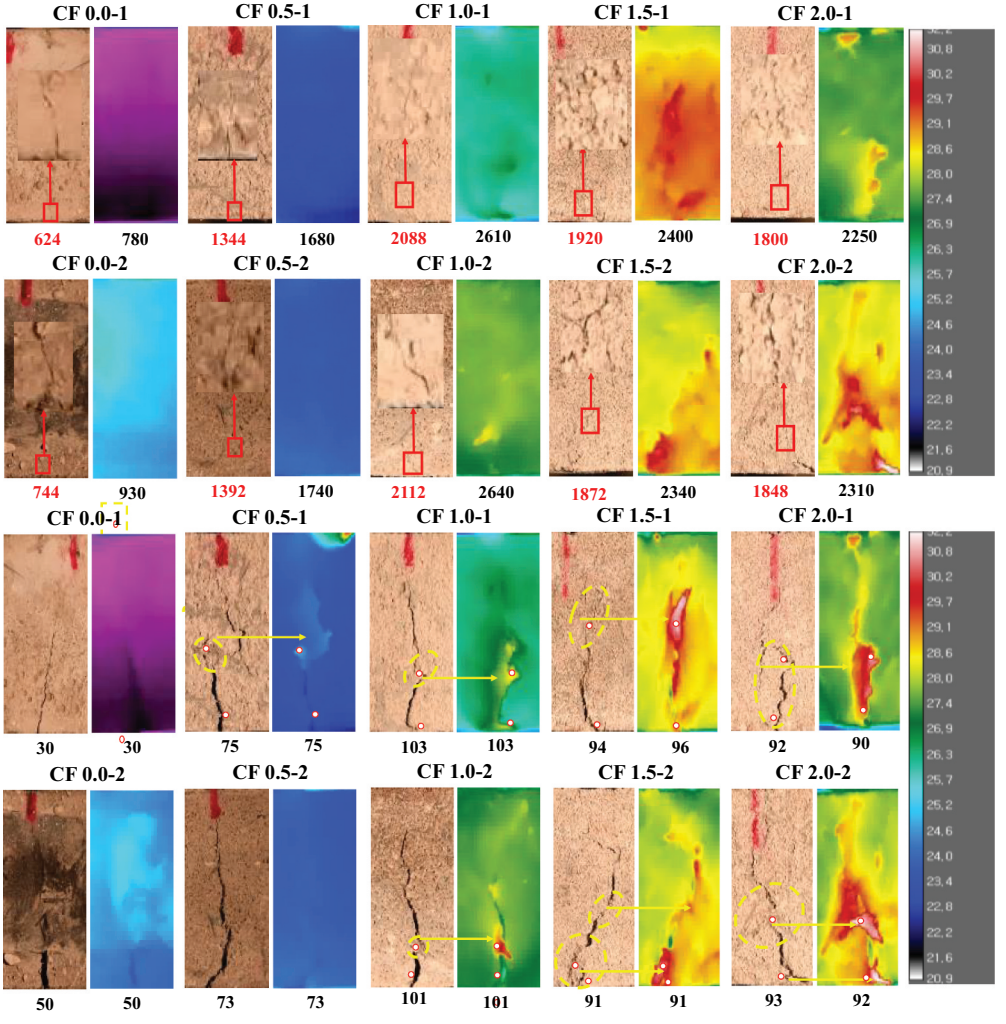

Figure 6. The comparison between the crack images in panchromatic and thermal cameras at the times of the crack on-set (1st and 2nd rows) and the moment when the forces from UTM is near vanished (3rd and 4th rows) for all prisms. The numbers in bottom of each prism image represents its frame number in the video for the 1st and 2nd rows, and the time it was taken for the 3rd and 4th rows: (a) the panchromatic images in the 1st and 2nd rows show the magnified images of the crack with 1 pixel width. The solid rectangle in each image specifies the location of the crack with 1 pixel width and its magnified image is above the arrow originated from the rectangle. The thermal images do not show the crack location but the patterns drawn by the colors for CF 0.5-1, CF 1.0-1(2), CF 1.5-1(2) and CF 2.0-1(2) will predict the possible path of the crack opening because of their close similarity to their corresponding thermal images in the 3rd and 4th rows. (b) When crack is widened as shown in the panchromatic images in the 3rd and 4th rows, the corresponding thermal images also reveal the crack path. The upper white dot in each of CF 0.5-1, CF 1.0-1(2), CF 1.5-1(2) and CF 2.0-1(2) is along the path of the crack opening. Its temperature is the highest in each image. The dot is a part of the fibers along the path. The fibers are specified by an broken ellipse in panchromatic image and its thermal image pattern is specified by the arrow.

The comparison between the crack images in panchromatic and thermal cameras. The numbers in bottom of each prism image represents its frame number in the video for the 1st and 2nd rows, and the time it was taken for the 3rd and 4th rows: (a) The 1st and 2nd rows' images are at the times of the crack on-set. (b) The 3rd and 4th rows' images are at the moment when the forces from UTM is near vanished.

are not defined sharply but their shapes are almost the same as those shown in the broken lined boxes. For the case of the CF 0.5-1. the right (left)-side edges along the white area in the thermal image follow closely the crack path in the right (left) box. There are two white circular dot with red edge (it will be named as a white dot) in Figure 6. The upper white dot in each prism represents the point revealing the highest temperatures due to the presence of the aggregated carbon fibre bundles and the bottom dot a point in no aggregated carbon fibre bundles at the bottom of the prism, but very near to the crack starting position. However, the upper white dot in each of the CF 0.0 and CF 0.5-2 is randomly chosen because of the absence of high-temperature areas along the crack path.

The aggregated fibres specified by broken ellipse in CF 1.5-1, CF 1.5-2, CF 2.0-1 and CF 2.0-2 are bigger than those in CF 0.5-1, CF 1.0-1, CF 1.0-2, CF 1.5-1, and that CF 1.5-2. The highest temperature area is specified by the white dot within the broken ellipse of each prism. This area is a part of the aggregated fibres along the crack path of each prism. As specified in CF 1.5-1 and CF 2.0-2 with the arrow, there is an aggregated fibres along the crack path in near the bottom of each of these prisms. These fibres should be stressed more than those in the broken ellipse in CF 1.5-1 and CF 2.0-2. However, these fibres are much smaller than those specified by the broken ellipses. This will be the reason why their temperature is lower than those in the broken ellipses. The fibres in the broken ellipses are those stressed mostly in each prism. However, it is considered that the fibres in CF 1.0-1 are not on the surface of the prism but underneath because of their lower temperature compared with those in CF1.5 and CF 2.0. The temperature is for the surface mortar that covers small aggregated fibres at its under.

For the case of CF 2.0-2, the broken part is a part of large aggregated fibres as shown by the surrounding large red colour area in thermal image. The large bundles have slightly lower temperature than the fibres in the broken part. This means that the fibres in the broken part are stressed more than their neighbouring fibres even if they belong to the same body.

Another interesting feature of Figure 6 is the crack paths that are separated from each other as shown in the upper box of CF 1.5-1 and the box in CF 2.0-1. The bundles in these boxes are invisible but inducing two paths because they cover the actual crack paths underneath of them. Hence, the two crack paths are passing the fibre bundles boundary with the mortar part, at where they are held strongly by the surrounding mortar. This is why they reveal the highest temperature in the prisms where they are in.

The actual crack path will appear when the bundles are completely detached from the mortar part due to the complete break of the prisms. As shown in CF 1.5-1, the temperature of the bundles and its surrounding areas have red colour at the crack on-set time but when the crack is progressed more, the bundles turned to white due to the concentration of the force on them, while its surrounding mortar areas turn to yellow. The fibre bundles in the bottom box of CF 1.5-2, the box CF 2.0-1 and the upper box of CF 2.0-2 also show the similar pattern as the CF 1.5-1.

The presence of the carbon fibre bundles in the prisms, especially along the crack path will be identified and detecting the crack path earlier than the actual crack appearing can be done with the thermal images. The thermal image at the crack on-set time has a very similar temperature distribution to that at the force vanishing moment. This similarity implies that the areas where the crack will be formed, are more stressed before the appearing of the actual crack in each prism. The fibre bundles along the crack path shows

their battle against further widening of the crack. But their resistance will last a short time period when they are too small to be easily detached from the mortar part.

Figure 7 shows the temperature variations at the points specified by two white dots in each prism in Figure 6. As shown in Figure 7, the temperatures in the upper (solid line) and lower (dotted line) white dots for CF 0.0 and CF 0.5-2 vary uniformly by keeping their differences to almost the same. For other prisms, the temperatures of both upper and lower white dots are also uniformly increasing as in the above three prisms, however, that of the upper white dot records a sudden increase in the temperature gradient at a certain moment. The arrow in each graph indicates the time point where the gradient changes are recorded. The values in the left and right sides of the arrow indicate the slopes before and after the changes. The ratio of the right to left values is in the range of 1.4 (CF 2.0-2) to 4.8 (CF 1.0-2). For the case of CF 2.0-2, the arrow indicates the 2nd increasing time point.

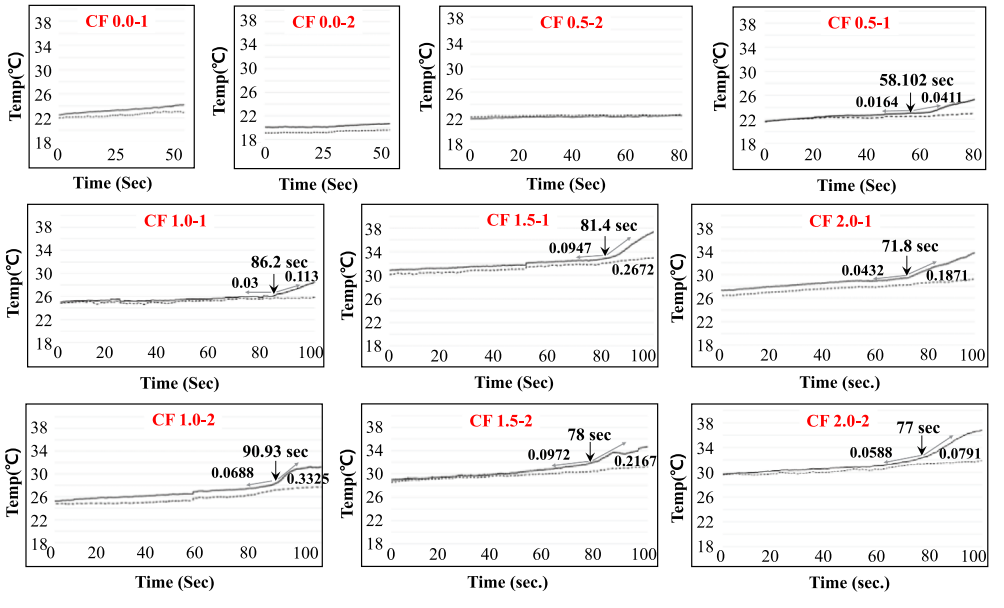

Figure 7. Temperature variations at the points specified by two white dots at each prism in Figure 6. The temperature variations for upper white dot are represented by solid lines and the lower by dotted lines. Temperature gradient changes are shown only on the solid lines, i.e. upper white dot temperature variations. The arrow in each graph indicates the time point where the gradient changes are recorded. The numbers in the left and right sides of the arrow indicate the slopes of before and after the changes. (a) for lower white dots no temperature gradients are shown. (a) for CF 0.0-1(2) and CF 0.5-2 do not show any temperature gradient because no fibers are on the crack paths. (b) for the case of CF 0.5-1, two gradient changes appear on the curve. The first gradient changes is almost unnoticeable but the time at its change is very close to the crack on-set time estimated from its corresponding panchromatic image. For other prisms, the gradient changes are very visible and their changing moment matches closely to the crack on-set time estimated from their panchromatic images.
Temperature variations at the points specified by two white dots at each named prism in Figure 6: The solid line curves which show the temperature gradient changes are for the upper white dot and the dotted line curves for the lower white dots. The arrow in each graph indicates the time point where the gradient changes are recorded. The numbers in the left and right sides of the arrow indicate the slopes of before and after the changes.

The sudden increase in the temperature gradient implies the stress concentration on the forefront fibre bundles, i.e. on the fibre bundles along the crack path of each prism. The mortar parts cannot bear the radially propagating stress from UTM when the crack is started because the prism is almost separated into two parts. But the forefront fibre bundles are still holding the two separated parts to resist to the further widening of the crack until they are completely detached from the mortar part. This is why the stress from the UTM becomes more concentrated on the forefront fibre bundles. Hence, the time at sudden temperature gradient increase will inform when the stress from the UTM will concentrate solely on the forefront fibre bundles. The time in second at the sudden gradient increase is 58.1 (56.0), 86.2 (87.0), 90.9 (88.0), 81.6 (80.0), 79.6 (78.0), 71.8 (75.0) and 77.0 (77.0) seconds for CF 0.5-1, CF 1.0-1, CF 1.0-2, CF 1.5-1, CF 1.5-2, CF 2.0-1 and CF 2.0-2, respectively, as shown in Table 1.

The numbers in the parenthesis are the corresponding crack on-set time determined by the panchromatic camera. The times showing the sudden gradient increase are somewhat higher than their corresponding crack on-set ones. But the differences between them are less than 3 seconds. When the time values for prisms with the same fibre percentage are averaged, they are (crack on-set time by the panchromatic) become 58.1 (57.5), 88.5 (88.5), 80.6 (79.0) and 74.4 (76.0) seconds for CF 0.5, CF 1.0, CF 1.5 and CF 2.0, respectively. The differences in these two values become less than 2 seconds, i.e. slightly above 2% (1.6/76) difference between them. The 2-second time difference can be considered as within the anticipated shuttering time mismatch between the two cameras. Hence, it can be said that the forefront fibre bundles start to bear most of the stress from the UTM at or very near to the moment of crack on-set. Measuring the time variation of the temperature at a point on one of aggregated carbon fibre bundles along the crack path will allow predicting the crack on-set time with the accuracy obtainable with a high-resolution panchromatic camera.

5. Conclusions

The carbon fibres added to the prisms not only increase the flexural strength of the prisms more than that of plain prisms, but also allow visualising the physical phenomenon involved in the crack developing process, estimating the crack path earlier than it actually appears, and determining the crack on-set time with high accuracy. These visualisation, estimation and determination can be done with the time variation of temperature distribution at the carbon fibres on the surface or slightly underneath the surface, along the crack path. The on-set time is determined by the point of inflection in the time variation of temperature distribution curve. At this inflection point, the gradient of the temperature distribution curve increases in 1.4 to 4.8 times of that of before the point, and the time at the inflection point of each prism matches to less than 2.2% differences with the crack on-set time determined by the video image obtained with a high-resolution panchromatic camera, for all the 7 prisms with different fibre amounts. Since the gradient is indifferent to the emissivity and thermal reflection from other objects in near the prism samples, it will not be affected by surrounding noises. The crack on-set time also matches to the sharp decreasing moment after the peak force time in the force waveform of the UTM.

The temperature distribution reveals also the aggregated locations of carbon fibre bundles and the uniform increase in the surface temperature of the prism as the forces from the UTM increase.

Disclosure statement

No potential conflict of interest was reported by the author(s).

Funding

This work was supported by Priority Reseach Centers Program through the National Reseach Foundation of Korea (NRF) funded by the Ministry of Education (Grant Number : NRF-2018R1A6A1A03025542).

References

[1] Sircas Jr GF, Adeli H. Infrared thermography for detecting defects in concrete structures. J Civ Eng Manage. 2018;24(7):508–515.
[2] Su T-C. Assessment of cracking widths in a concrete wall based on TIR radiances of cracking. Sensors. 2020;20(17):4980.
[3] Masato M, Mitani K, Catbas FN. Bridge assessment methods using image processing and infrared thermography technology. Proceedings of 92nd Annual Meeting; 2013; Japan.
[4] Tashan J, Al-Mahaidi R. Detection of cracks in concrete strengthened with CFRP systems using infra-red thermography. Composites. 2014;64:116–125.
[5] Kylili A, Fokaides PA, Christou P, et al. Infrared thermography (IRT) applications for building diagnostics: a review. Appl Energy. 2014;134:531–549.
[6] Rocha JHA, Póvoas Y. Detection of delaminations in reinforced concrete bridges using infrared thermography. Revista Ingeniería de Construcción. 2019;34(1):55–64.
[7] Garrido I, Laguela S, Arias P. Infrared thermography's application to infrastructure inspections. J Infrastruct. 2018;3(35):1–19.
[8] Toutanji HA, El-Korchi T, Katz RN. Strength and reliability of carbon-fiber-reinforced cement composites. Cem Concr Compos. 1994;16(1):15–21.
[9] Pinson L-J, editor. Electro-Optics. New York: John Wiley and Sons; 1985. Chapter 2, Optical Radiation;p. 21–31.
[10] FLIR. 2020. Available from: https://www.flir.com/browse/industrial/handheld-thermal-cameras/.
[11] UTS. 2020. Available from: https://www.testresources.net/test-machines/universal-testing-machines.
[12] Nikon. 2020. Available from: https://www.nikonusa.com/en/nikon-products/product/dslr-cameras/d5.html#tab-ProductDetail-ProductTabs-TechSpecs.
[13] ASTM C 1161-02C (2008)e1Standard test method for flexural strength of advanced ceramics at ambient temperature. West Conshohocken, PA: ASTM International.
[14] Daniels A. Field guide to infrared systems, detectors, and FPAs. 3rd ed. Vol. FG40, Bellingham, Washington, USA: SPIE Press; 2018.
[15] Heo G, Kim J, Yim C, et al. Carbon fiber traces in cracked surfaces of mortar prisms. Appl Sci. 2022;12(4):2110.